RESEARCH MEMORANDUM

ZERO-LIFT DRAG OF A SERIES OF BOMB SHAPES AT MACH NUMBERS FROM 0.60 TO 1.10

By William E. Stoney, Jr., and John F. Royall

Langley Aeronautical Laboratory
Langley Field, Va.

NATIONAL ADVISORY COMMITTEE
FOR AERONAUTICS

WASHINGTON

July 26, 1956

NACA RM L56D16

NATIONAL ADVISORY COMMITTEE FOR AERONAUTICS

RESEARCH MEMORANDUM

ZERO-LIFT DRAG OF A SERIES OF BOMB SHAPES AT MACH NUMBERS FROM 0.60 TO 1.10

By William E. Stoney, Jr., and John F. Royall

SUMMARY

Zero-lift drag data were obtained on a series of six bomb shapes. Five configurations had the same body shape, the only difference being in the body-surface conditions and the profile and plan form of the fins, while the sixth configuration had a different and longer body shape. The models were launched from a helium gun (at the Langley Pilotless Aircraft Research Station at Wallops Island, Va.), and data were obtained for Mach numbers from 0.60 to 1.10 with corresponding Reynolds numbers based on body length of 5×10^6 to 10×10^6.

It was found that at subsonic speeds the blunt trailing edge of the fins contributed a large share of the drag while the effect of the blunt leading edge was negligible. Two models whose roughness did not exceed 20 rms microinches had measurably lower subsonic drag coefficients than the remaining models whose roughness varied between 100 and 250 rms microinches.

INTRODUCTION

The Langley Pilotless Aircraft Research Division has conducted zero-lift drag tests on a series of bomb models. The object of the tests was to determine the subsonic drag level of a proposed configuration. When this original configuration proved to have too high a subsonic drag, attention was turned to determining the means and the efficacy of the means to be used to reduce the subsonic drag level. The test program is reported herein. The models were launched from a helium gun at the Langley Pilotless Aircraft Research Station at Wallops Island, Va.

SYMBOLS

M	Mach number
q	dynamic pressure
C_D	total drag coefficient, $\frac{\text{Total drag force}}{q \times \text{Maximum frontal area}}$
C_{D_b}	base drag coefficient
C_{D_f}	friction drag coefficient
L	length
D	maximum diameter
rms	root mean square
R	Reynolds number, based on model length or fin mean chord

MODELS AND TESTS

The test configuration dimensions are shown in figure 1, photographs appear in figure 2, and the drawing ordinates are given in tables I(a) and I(b). All of the models were measured and found to be within ±0.016 inch of the desired dimensions. The maximum diameter, 2.598 inches, and the total body length, 14.64 inches, were the same for each of the first five configurations, while the sixth configuration had a maximum diameter of 3.00 inches, and 20.50 inches was the total body length.

The models have been divided into six configurations (a to f). Two essentially identical models of configurations a and f were flown and these are noted simply as models 1 and 2 for both configurations.

A description of each configuration is shown in table II, together with the surface measurements. These measurements were made with a small portable profilometer (trade-marked Type Q, Physicists Research Co.).

The models were fired from a helium gun at Wallops Island, Va. (The helium gun makes use of the rapid release of compressed helium to propel the models into free air at a Mach number of about 1.1.) Velocity data were obtained as the models decelerated by the use of a CW Doppler velocimeter which was located on the ground next to the helium gun. Total drag coefficients were determined from the measured velocity together with the variation of density, temperature, and wind velocity with altitude obtained by a radiosonde survey made about the time of firing. These measurements are estimated from experience with previous models to be accurate within ± 0.01 in C_D and ± 0.01 in M.

Data were obtained over a range of Mach numbers from 0.60 to 1.10 and for Reynolds numbers based on body length from 5×10^6 to 10×10^6.

RESULTS AND DISCUSSION

The drag coefficients for the test models are presented as functions of Mach number in figure 3, with the coefficients based on maximum body frontal area ($\pi D^2/4$). The results are of interest primarily at the Mach numbers below 0.90. The various configurations are compared to show the effects of the following test variables: leading- and trailing-edge bluntness, fin thickness, and body-surface roughness. Though the models were rolling at an unknown rate (note 2° incidence of two fins of configurations a to d and unsymmetrical fin profile of configurations e and f), no attempt has been made to evaluate the influence of the rolling rate on the drag. It seems reasonable to assume, however, that all the models of series a to d and series e and f rolled at approximately equal rates, but the two groups may have had somewhat different rates of roll.

Effect of Blunt Trailing Edge

The subsonic drag levels of both configuration a models (which had blunt-trailing-edge fins) were considerably higher than those of the remaining models, all of which, with the exception of configuration e, had fins with sharp trailing edges (fig. 3(a)). The trailing edge of the configuration e was thin enough (approximately 1/4 of that of configuration a) so that it may be taken as sharp for the purposes of this report. The drag difference between the a models and the remaining models may be attributed directly to the base pressure on the blunt fins. If the base pressures of reference 1 and the ratio of the model fin base area to body frontal area are used, the resulting C_{D_b} is approximately 0.06, which is about the difference shown in figure 3(a) between model 2 of configuration a and configuration c. The difference between models 1 and 2 of configuration a may be due partly to differences in fin base area (due to construction inaccuracies) and partly to test inaccuracy.

Effect of Blunt Leading Edge

Comparisons of the data (fig. 3) of configurations b (sharp leading edge) and c (blunt leading edge) indicate that the drag increase caused by the blunt leading edge was small.

Effect of Fin Thickness

Although the fins of configuration e are of different plan form than those of the other short models, it seems reasonable to assume that the major cause of the higher drag-rise Mach number of this model is the thinness of its fins, that is, 0.046 inch compared with 0.16 inch. Since the drag increases shown by all the configurations are approximately equal, it is probably not the increased drag rise of the thicker fins themselves that causes the early drag rise of the thick-finned models but rather the greater interference of the fins with the body which, in turn, causes the early drag rise of the body itself.

Effect of Body Surface

All of the models presented in figure 3(a) except configuration d were in the original "as cast" condition. Configuration d was sanded to approximately 30 to 40 rms microinches over the nose and over scattered sections of the remaining parts of the model. A comparison of the data for configurations b and d indicates that as far as drag is concerned the body surfaces are equally rough. That even the smoothest model (configuration d) was far from aerodynamically smooth is indicated by the comparison of the data with the two calculated friction-drag points at $M = 0.7$ and $M = 0.9$. These points were calculated by the method of Van Driest (ref. 2), with the assumption of turbulent flow over the entire lengths of both body and fins. Since at subsonic speeds there is no pressure drag other than that caused by separated flow regions, most of this difference between theoretical and measured subsonic drag may be assumed to be due to the effect of the surface roughness on the level of the turbulent-friction-drag coefficient. At least a qualitative idea of this effect may be gained from the chart on page 44 of reference 3 which shows the dependency of the turbulent skin friction on grain size.

The presence of this effect in the data of all the models of figure 3(a) is shown by the better agreement of theoretical and measured drag in figure 3(b). The two models of configuration f, while longer, were considerably smoother all over than the smaller models. This is shown in table II which mentions that configuration f had a maximum roughness of 20 rms microinches, while the smoothest of the short models had considerable areas with roughness of 80 to 160 rms microinches. The effect of this surface roughness on the friction drag is shown by comparison with the theoretical calculations of reference 2. At $M = 0.7$, the fin

Reynolds number based on mean aerodynamic chord is about 1×10^6 and thus a C_{D_f} value based on laminar flow for the fin is also presented.

CONCLUSIONS

Tests on a series of bomb shapes flown at Mach numbers from 0.60 to 1.10 and body length Reynolds numbers of 5×10^6 to 10×10^6 indicate the following effects of configuration change on zero-lift drag:

1. At subsonic speeds the blunt trailing edge contributed a large share of the drag.

2. The effect of a blunt leading edge was relatively small in comparison with drag caused by the blunt trailing edge.

3. The subsonic drag showed no change attributable to roughness in the range of roughnesses of 100 to 250 rms microinches. Two models whose maximum roughness did not exceed 20 rms microinches had measurably lower subsonic drag levels.

Langley Aeronautical Laboratory,
National Advisory Committee for Aeronautics,
Langley Field, Va., March 30, 1956.

REFERENCES

1. Morrow, John D., and Katz, Ellis: Flight Investigation at Mach Numbers From 0.6 to 1.7 To Determine Drag and Base Pressures on a Blunt-Trailing-Edge Airfoil and Drag of Diamond and Circular-Arc Airfoils at Zero Lift. NACA TN 3548, 1955. (Supersedes NACA RM L50E19a.)

2. Van Driest, E. R.: Turbulent Boundary Layer in Compressible Fluids. Jour. Aero. Sci., vol. 18, no. 3, Mar. 1951, pp. 145-160, 216.

3. Hoerner, Sighard F.: Aerodynamic Drag. Publ. by the author (148 Busteed, Midland Park, N. J.), 1951.

TABLE I.- DRAWING ORDINATES OF CONFIGURATIONS

(a) Configurations a, b, c, d, and e

Station, in.	Radius, in.
0	0
.12	.315
.28	.476
.44	.585
.70	.787
.935	.833
1.170	.914
1.400	.981
1.640	1.046
2.440	1.190
2.840	1.235
3.240	1.271
3.640	1.287
4.040	1.299
6.200	1.299
6.90	1.289
7.60	1.259
8.31	1.210
9.02	1.142
10.42	.947
11.134	.836
11.839	.706
12.160	.642
12.544	.563
13.249	.417
13.954	.271
14.521	.153
14.640	0

(b) Configuration f

Station, in.	Radius, in.
0	0.529
.100	.608
.165	.656
.300	.736
.600	.886
.665	.916
1.100	1.071
1.165	1.093
1.600	1.208
1.665	1.225
2.040	1.300
2.165	1.325
2.520	1.378
2.665	1.393
2.980	1.432
3.165	1.453
3.440	1.470
3.665	1.486
4.165	1.498
4.240	1.499
4.365	1.500
10.762	1.500
11.576	1.488
12.388	1.454
13.201	1.397
14.015	1.319
14.829	1.200
15.642	1.095
16.454	.966
17.638	.742
18.895	.481
19.709	.313
20.363	.176
20.500	0

TABLE II.- CONFIGURATION DETAILS

Configuration	Fin leading edge	Fin trailing edge	Body-surface condition	Body-surface measurements, rms microinches
a (models 1 and 2)	Blunt	Blunt	Rough	Nose - 80 to 130 Body - 140 to 250 Fins - 40 to 60
b	Sharp	Sharp	Rough	Same as configuration a
c	Blunt	Sharp	Rough	Same as configuration a
d	Sharp	Sharp	Smooth	Nose - 30 to 40 Body - 40 to 50 (smooth sections) 80 to 160 (rough sections) Fins - 30 to 35
e	Blunt	Blunt	Rough	Same as configuration a
f (models 1 and 2)	Blunt	Blunt	Smooth	Body and fins - 16 to 20

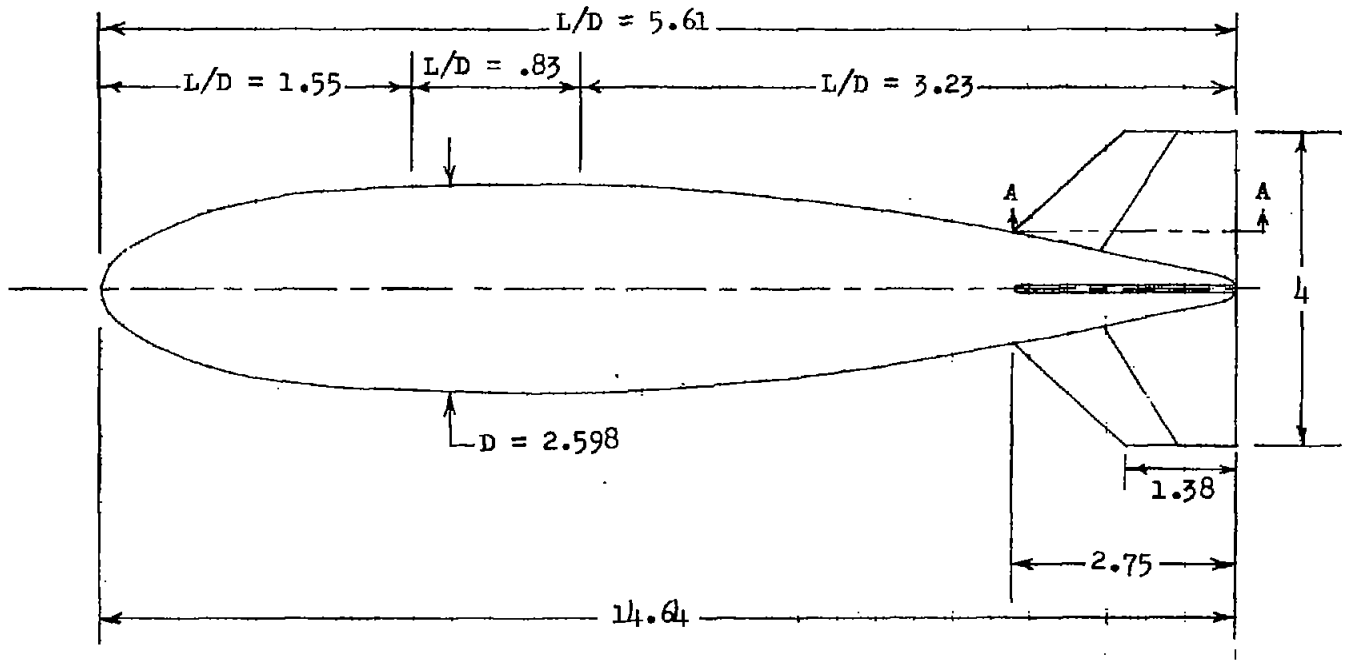

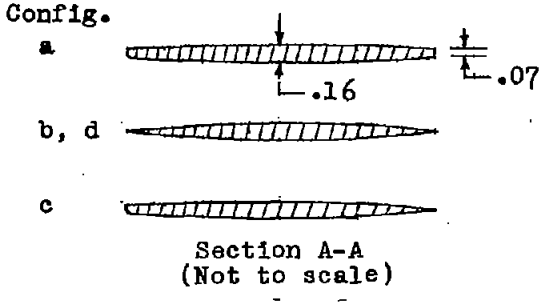

Note- 2 fins set at about 2° incidence.

(a) Dimensions of configurations a, b, c, and d.

Figure 1.- Test configurations. (All dimensions are in inches.)

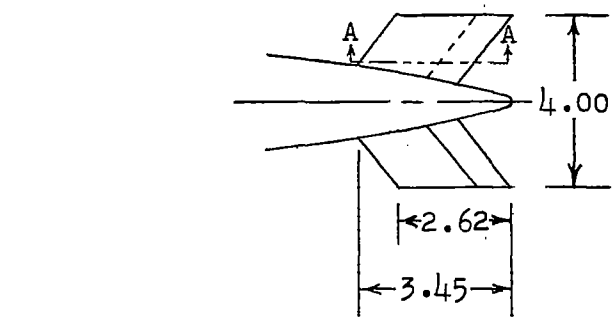

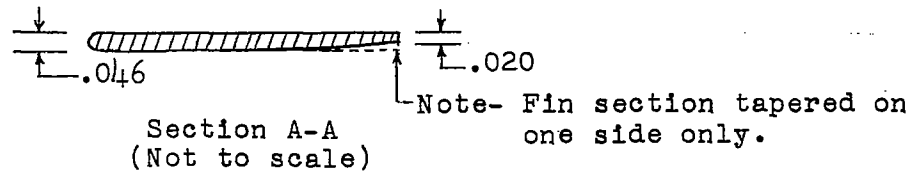

Section A-A
(Not to scale)

(b) Dimensions of configuration e (body dimensions same as for configurations a, b, c, and d).

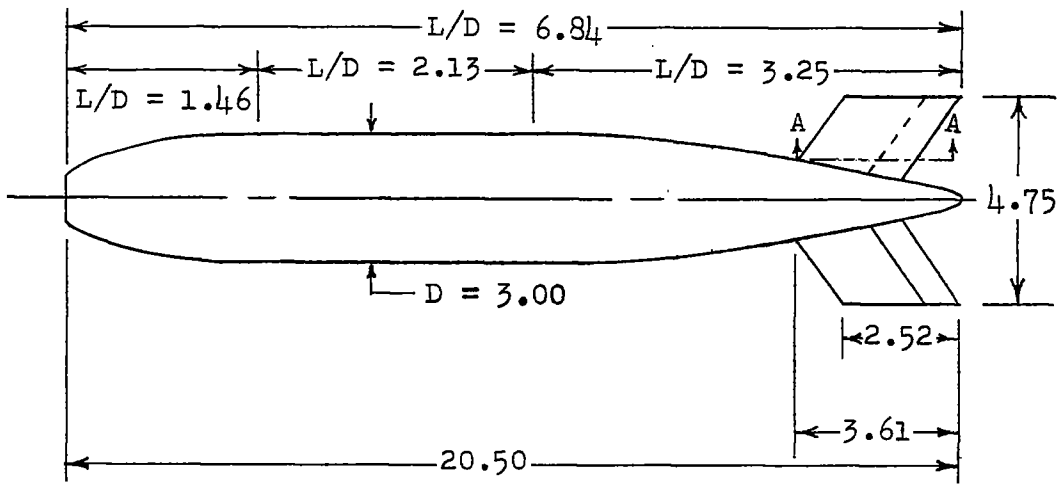

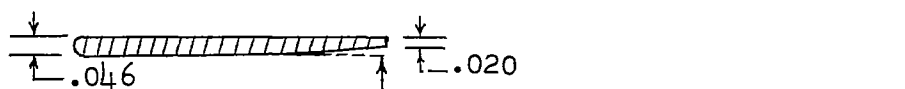

Section A-A
(Not to scale)

(c) Dimensions of configuration f.

Figure 1.- Concluded.

(a) Configurations a, b, c, and d.

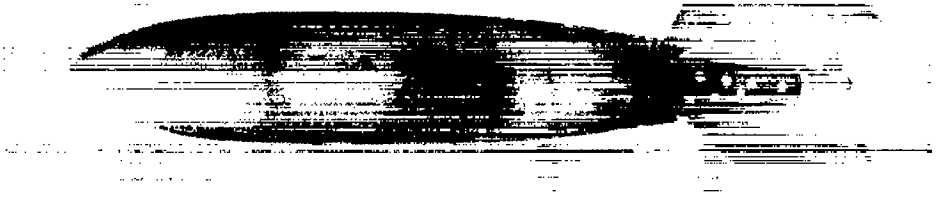

(b) Configuration e.

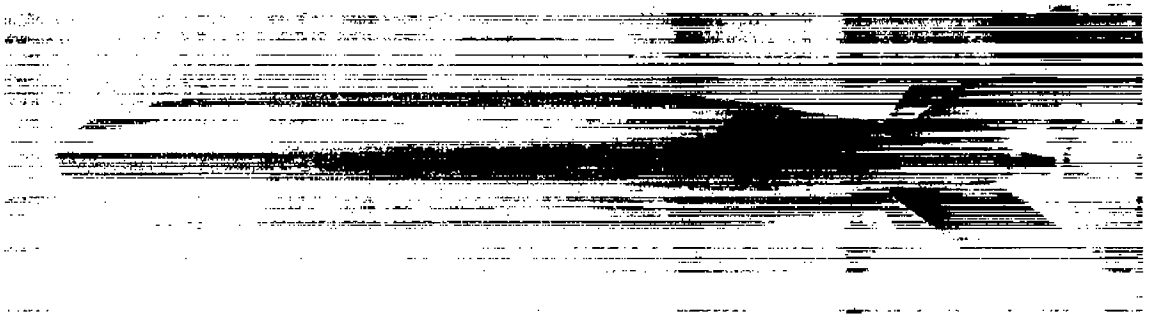

L-92473

(c) Configuration f.

Figure 2.- Photographs of models.

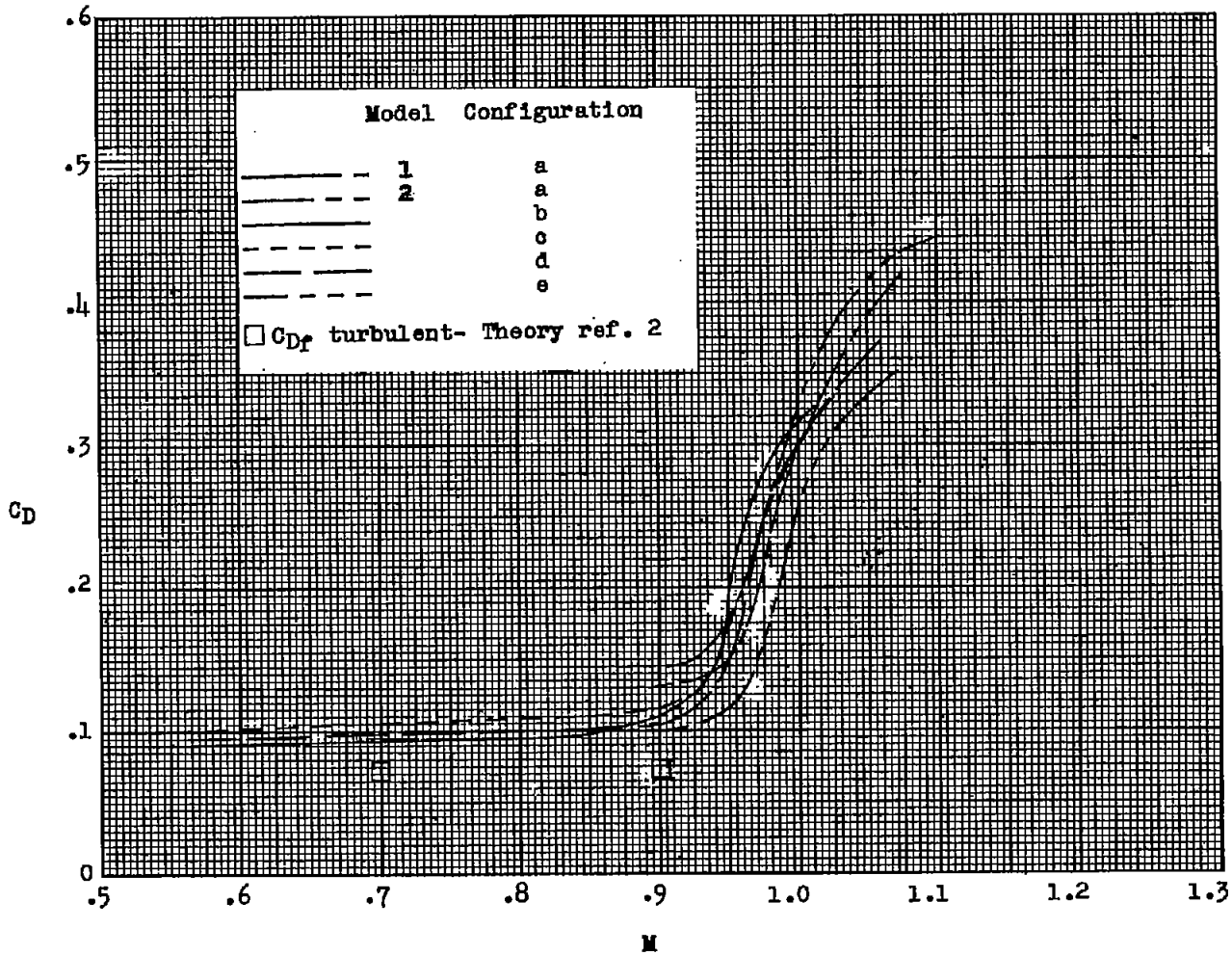

(a) Configurations a, b, c, d, and e.

Figure 3.- Drag coefficients as a function of Mach number for test configurations.

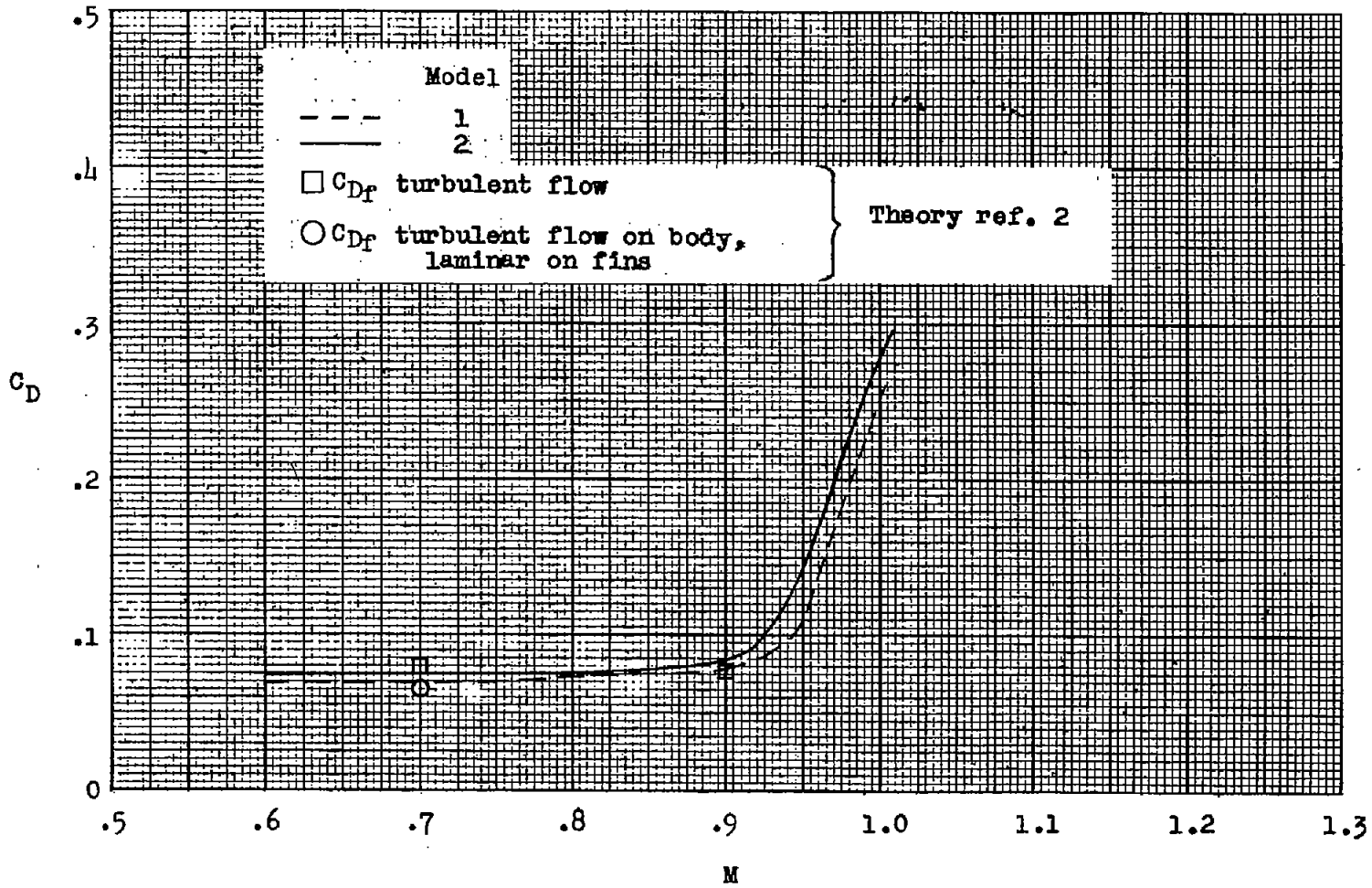

(b) Configuration f.

Figure 3.- Concluded.